Optical Second Harmonic Generation Study of Malachite Green Orientation and Order at the Fused-Silica/Air Interface

Tanya Kikteva, Dmitry Star, and Gary W. Leach*

Department of Chemistry, Simon Fraser University, 8888 University Drive, Burnaby, British Columbia V5A 1S6 Canada

Received: August 2, 1999; In Final Form: December 9, 1999

Optical second harmonic generation (SHG) studies of malachite green (MG) adsorbed at the fused-silica/air interface have been conducted. The concentration dependence of the second harmonic intensity indicates the formation of ordered monolayers normal to the interface. Polarization SHG experiments have been used to extract the averaged molecular orientation in adjacent molecular layers and to characterize the breadth of the orientation distribution. MG adsorbs in an upright orientation with its molecular plane near normal to the surface. This orientation is consistent with the interaction of the polar surface and the polar dimethylamino substituents of the adsorbate. Molecular orientation in the second monolayer resembles that in the first, but also reflects some additional broadening of the orientation distribution function. The onset of parallel, sandwich-type aggregates has been observed within the first monolayer. The formation of parallel, sandwich-type, *intralayer* aggregates is distinct from the *interlayer* aggregation observed between adjacent monolayers of rhodamine 6G. These differences result from the nature of the molecule−surface interactions that define their respective orientations in the first monolayer. Thus, it appears that the order observed in these ultrathin organic films is dictated by the molecule−surface interactions within the first monolayer as well as the magnitude of the intermolecular interactions in subsequent layers.

I. Introduction

The characteristics of ultrathin organic films are currently attracting much attention because of their promise as a versatile and inexpensive means of constructing molecular-based devices. The unique optical and electronic properties of organic systems have been exploited to produce devices ranging from light-emitting diodes,[1,2] thin film conducting devices,[3,4] and chemical sensors,[5,6] to field-effect transistors.[7,8] One observation that has arisen from such studies is that the luminescence and carrier mobility characteristics of these device prototypes are strongly linked with the structure and crystallinity of the organic active layers. Thus, an understanding of what factors affect molecular order in organic films may also be exploited for its control and potentially be used to optimize device performance.

In a previous publication we have presented results describing the orientation, aggregation, and ordering of the organic dye molecule rhodamine 6G (RGG) at the fused-silica/air interface in an effort to understand the factors affecting the structure of ultrathin organic films.[9] In that study we established that the organic probe molecule interacts with the substrate through its polar functional groups and is adsorbed with an orientation such that its primary interactions within the first monolayer are adsorbate−substrate in nature. Subsequent adsorption leads to the formation of interlayer aggregates with antiparallel averaged molecular orientations in adjacent layers. As a result of these intermolecular interactions, molecular ordering normal to the surface persists for approximately five molecular adlayers before orientational anisotropy is lost. Here, we describe results for the probe molecule malachite green (MG), and show that the molecular ordering observed for rhodamine films appears to be a general phenomenon. However, the details of the averaged molecular orientation within each adlayer, as well as the nature and degree of aggregation and order, are system-dependent, determined by the details of the adsorbate−substrate and adsorbate−adsorbate interactions.

MG has been the subject of considerable interest and investigation over the past two decades, in part because of its use as a saturable absorber used to generate ultrashort laser pulses and also in an effort to understand the details of its unusual excited-state photophysics. MG displays an unusually short excited-state lifetime, which in solution is solvent viscosity-dependent. Numerous studies using a variety of techniques[10−15] have shown that upon excitation to its first excited singlet state, MG undergoes a rapid nonradiative decay process linked with internal rotation of its phenyl groups. This photoinduced isomerization results in observed fluorescence and ground-state recovery lifetimes on the picosecond time scale. More recently, the excited-state dynamics of MG adsorbed on silica have been investigated by picosecond time-resolved surface second harmonic generation (SHG).[16−18]

Here, we report the use of the surface-specific nonlinear optical technique of SHG[19−22] to elucidate the details of the orientation, aggregation, and ordering properties of MG at the fused-silica/air interface. Optical SHG relies on the broken symmetry inherent to the interface formed between bulk media possessing macroscopic inversion symmetry. Within the electric dipole approximation, the presence of intense electric fields at the noncentrosymmetric interface can give rise to even-order nonlinear optical effects, which are interface-specific. SHG, a second-order nonlinear response, has been exploited to examine surface and interface structure, providing information regarding adsorbate orientation in a variety of systems ranging in nature from the solid/air[23,24] to solid/liquid,[24,25] liquid/vapor,[24,26] and

* To whom correspondence should be addressed. E-mail: gleach@sfu.ca.

10.1021/jp992728b CCC: $19.00
Published on Web 03/11/2000

liquid/liquid[27−29] interfaces. The technique takes advantage of the second-order nonlinearity ($\chi_s^{(2)}$) inherent to the interface. An intense laser beam of frequency ω and polarization $\hat{e}_\omega$ incident on a surface or interface at an angle ϕ with respect to the surface normal will produce second harmonic (SH) light at frequency 2ω and polarization $\hat{e}_{2\omega}$ with an intensity given by[30]

$$I_{2\omega} = 32\pi^3 \left(\frac{\omega^2}{c^3}\right) \sec^2 \varphi |\hat{\mathbf{e}}_{2\omega} \cdot \chi_s^{(2)}(2\omega) : \hat{\mathbf{e}}_\omega \hat{\mathbf{e}}_\omega|^2 I_\omega^2 \qquad (1)$$

Under conditions where the macroscopic second-order susceptibility is dominated by the presence of the adsorbed molecules, the susceptibility tensor, $\chi_s^{(2)}$, can be written in terms of an average of the individual nonlinear molecular polarizability contributions, $\beta^{(2)}$:

$$\chi_s^{(2)} = N_s \sum \langle \beta^{(2)} \rangle \qquad (2)$$

where N_s is the number of adsorbed molecules on the surface, and the brackets denote an average taken over all adsorbate orientations. Note that this expression neglects substrate contributions to the nonlinearity and local field effects that result from spatial variations of the local field because of molecule−surface and molecule−molecule interactions and from contributions of the dipole fields of other polarized surface molecules. Measurement of the macroscopic susceptibility tensor components combined with some knowledge regarding the electronic structure of the adsorbate can then be used to provide information regarding the averaged molecular orientation.

In this report we describe optical SHG and absorbance studies of the cationic dye molecule MG, spin-cast on fused silica. In Section II we describe the method of film deposition and the experimental apparatus used to carry out these studies. After this, we present the results of our surface SHG experiments, which indicate well-defined order in successive adsorbate layers and the method used to determine the averaged molecular orientation within the layers. Next, we describe the results of absorbance measurements carried out on these films in the context of molecular aggregation. Our work is summarized in Section IV.

II. Experimental Section

A detailed description of the apparatus used to conduct the optical SHG measurements has been presented recently,[9] so only a brief description is given here. SHG measurements of MG adsorbed at the fused-silica/air interface were carried out in a total internal reflection geometry using the regeneratively amplified output of a mode-locked titanium:sapphire oscillator. This system is capable of producing 100-fs pulses with an energy of 1 mJ, tunable from 750 to 850 nm. Only a small fraction (typically <10 mW) of the available laser power was used during these studies. The polarization of the incident pulses was controlled by passing them through a quartz zero-order half-wave plate, followed by a polarizer to ensure polarization purity. The incident beam is then passed through an interference filter before striking the interface to filter any SH light that may be generated at previously encountered mirror interfaces or in the quartz half-wave plate.

We use a right-angle, optical-quality, fused-silica prism as a substrate because large signal enhancements can be obtained when these types of experiments are carried out in conditions of total internal reflection.[27,33] The 800-nm light is directed at near-normal incidence on the small face of the right-angle prism to achieve a condition of total internal reflection on the prism hypotenuse. The SH light generated at this interface propagates through the prism and exits at approximately a right angle to the incident fundamental light. Note that because of the wavelength difference between the incident fundamental and generated SH light, the two beams propagate at slightly different angles through the prism and can be spatially separated quite readily. The fundamental and generated SH light are then spatially filtered, passed through a filter designed to block the fundamental wavelength, then a Glan−Taylor polarizer for polarization selection, and finally focused onto the entrance plane of a 0.25-m monochromator. The spectrally filtered light is collected with a photomultiplier tube and averaged with a boxcar integrator before being processed by an IBM-compatible personal computer.

Use of 800 nm as a fundamental wavelength led to the production of large surface SHG signals due to a two-photon resonance enhancement with the second excited electronic state of MG occurring at 410 nm. The wavelength dependence of the SH response indicated that the magnitude of the signal resonance enhancement was on the order of 300. As a result, use of lower fundamental light intensities still gave rise to excellent signal-to-noise levels while minimizing any multiphoton absorption-induced optical damage,[18] as determined by the time dependence of the SH signals.

Preparation of the interfaces was carried out by spin-coating of MG (Sigma) from ethanolic solutions. Surface coverage was varied by spin-coating solutions of varying concentration at a fixed spin speed of 1600 rpm for 5 min. Adsorbate surface coverage was determined with the aid of both the measured SH response and linear absorbance measurements. Film uniformity and quality were judged with an optical microscope. Using the spin-cast method, surface coverage reproducibility was observed to be approximately 95% even at coverages corresponding to fractions of a monolayer. This level of reproducibility was indicated for all concentrations investigated both by absorption and SHG measurements. Fluorescence measurements of the fused-silica substrates deposited with MG were attempted using a fluorometer with single-photon counting detection. This apparatus readily permitted the acquisition of fluorescence spectra for substrates with submonolayer coverages of R6G; however, no fluorescence from MG-coated substrates could be detected.

III. Results and Discussion

SHG Concentration Dependence. The concentration dependence of the SH response from MG-coated surfaces is illustrated in Figure 1a. The p-polarized optical SH response is plotted as a function of surface concentration. The surface concentration can be expressed in terms of the solution concentration from which the film was cast and also in units of molecules/cm^2, determined from the extinction coefficient of MG in ethanol solution and assuming that the adsorbate oscillator strength is the same as that in solution. The SH response increases rapidly with surface coverage up to a value of approximately 3.2×10^{14} molecules/cm^2. A closer examination of this coverage range indicates that the signal slope changes slightly and discontinuously at roughly half of this surface coverage (1.6×10^{14} molecules/cm^2). A third identifiable range between 3.2 and 5.0×10^{14} molecules/cm^2 displays a more pronounced change in slope, with the SH response increasing more modestly with surface coverage. At higher spin-coat concentrations the SH signal increases more rapidly again before reaching a plateau at $\sim 6.0 \times 10^{14}$ molecules/cm^2 and then

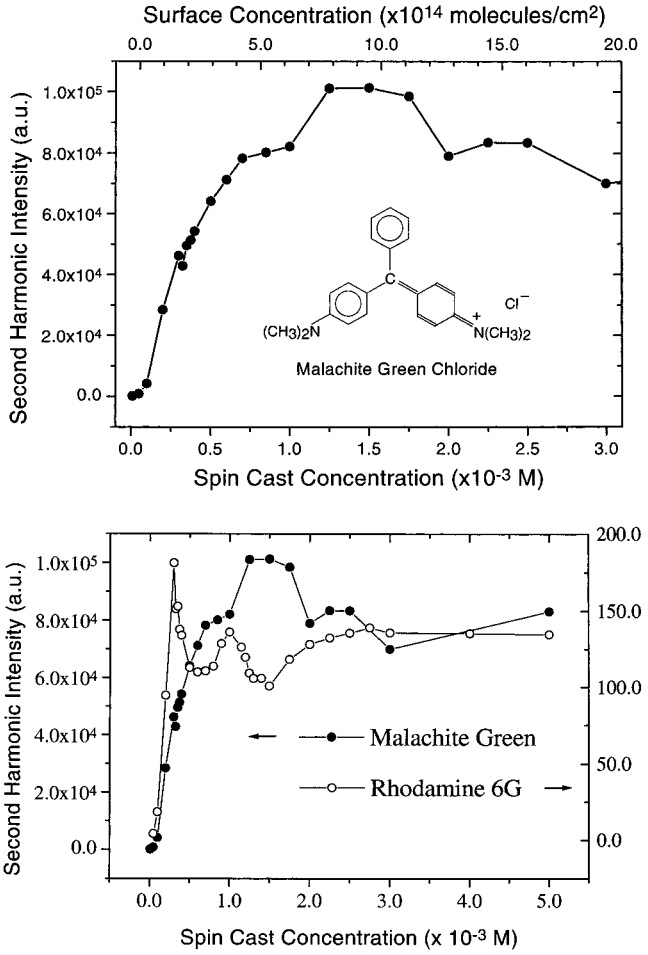

Figure 1. (a, top) Plot of second harmonic (SH) intensity versus malachite green (MG) surface concentration expressed in terms of the spin-coat concentration and as molecules/cm^2. (b, bottom) Comparison of the concentration-dependent SH intensity of MG (filled circles) and rhodamine 6G (open circles). See ref 9.

decreasing in magnitude at $\sim 9 \times 10^{14}$ molecules/cm^2. At higher concentrations still, the signal continues to show discontinuities in slope.

Equations 1 and 2 infer that for conditions of constant incident intensity, the magnitude of the SH signal is a measure of the surface susceptibility, $\chi_s^{(2)}$, dependent upon the number of molecules on the surface, their molecular nonlinear polarizabilities, and the averaged adsorbate orientation. Absorbance measurements of the MG films show a strictly linear dependence on surface coverage, indicating that the discontinuous nature of the concentration dependence must be attributed to concentration-dependent changes in the averaged molecular orientation. We have recently reported such coverage-dependent orientation observed in our examination of the organic dye molecule R6G. Figure 1b shows the concentration dependence observed in the case of R6G and for comparison, the (rescaled) concentration dependence of MG displayed in Figure 1a. We have shown that the oscillatory dependence observed for R6G reflects an interference effect between adjacent adlayers, which adsorb with approximately antiparallel geometries, and that the extrema observed in the SHG signal correspond to the completion of successive layers. Similarly, we assign the discontinuities observed for MG displayed in Figure 1 to the formation of successive MG adlayers. Indeed, Figure 1b indicates that there is a close correspondence between the surface coverages at which layer formation is completed for both probe molecules. Thus we attribute the break in slope at an MG surface coverage of 1.6×10^{14} molecules/cm^2 to the completion of one monolayer. Likewise, completion of two monolayers is observed at 3.2×10^{14} molecules/cm^2, twice the concentration required to achieve single monolayer surface coverage. A surface coverage of 1.6×10^{14} molecules/cm^2 (1.0 monolayer) corresponds to an area per molecule of ~ 60 Å^2. This is in close agreement with the value of 65 Å^2/molecule obtained for R6G.[9]

Our observations for MG indicate that the interference effect observed in the case of rhodamine is absent and that the similarity in slope between the first and second monlayers of MG reflect similar averaged orientations in the first two molecular layers. Further, the observation of well-defined slope changes in the concentration dependence of the SH signal is a signature of the formation of ordered layers normal to the surface. Figure 1b illustrates that this type of ordering seems to be quite a general phenomenon, at least for this class of molecule. However, it is also clear from Figure 1 that adsorbate orientation within an individual adlayer as well as the relative orientations in adjacent layers are distinct and molecule-dependent. To examine the adsorbate orientation and to elucidate the interactions responsible for the formation of the ordered layer structure, we have conducted polarized SHG studies.

SHG Polarization Dependence. We have examined the polarization dependence of the surface SH response to extract the elements of the second-order nonlinear susceptibility tensor $\chi^{(2)}$, and to obtain orientational information about the adsorbed molecules.[22] For a monolayer of molecules distributed randomly in the plane of the surface (defined to be the *XY* plane) the susceptibility tensor possesses only three unique elements: χ_{xzx}, χ_{zxx}, and χ_{zzz}. The values of these three components can be obtained by monitoring the polarization-selected SH intensity at frequency 2ω as a function of the polarization angle of the incident light at frequency ω. The expected incident polarization dependence of the polarization-selected SH signal intensity is given by:

$$I_\psi(2\omega) \propto |[c_1\chi_{xzx}\cos 2\gamma \sin 2\gamma]\sin\psi + [(c_2\chi_{xzx} + c_3\chi_{zxx} + c_4\chi_{zzz})\cos^2 2\gamma + c_5\chi_{zxx}\sin^2 2\gamma]\cos\psi|^2 I(\omega)^2 \quad (3)$$

where the polarization detection angle is labeled ψ, and $\psi = 0°$ and $\psi = 90°$ correspond to p-polarized and s-polarized SH intensities, respectively. We have used a $\lambda/2$ plate (waveplate angle γ) to control the polarization angle (2γ) of the linearly polarized incident beam. Thus, the incident electric fields are defined such that

$$E_p(\omega) = E(\omega)\cos 2\gamma \; E_s(\omega) = E(\omega)\sin 2\gamma \quad (4)$$

The constants c_i in eq 3 describe the magnitudes of the electric fields in the surface monolayer and are proportional to the Fresnel factors describing transmission and reflection at each interface encountered, as well as the appropriate dielectric constants for the materials used. The calculation of these constants has been outlined for a variety of different experimental geometries,[34] including the total internal reflection[33]-geometry used here. The values of the Fresnel factors and constants c_i used for our analysis have been calculated following the analysis of Felderhof et al.[33]

Figure 2 illustrates the observed incident polarization dependence of the polarization-selected SH intensity for a variety of detected polarization angles, ψ. The experimentally determined values of the SH intensity are displayed as individual points and the solid lines are fits to these data according to eq 3. The functional dependence of the s-polarized ($\psi = 90°$) SH response (Figure 2b) on the input polarization angle is a signature of the

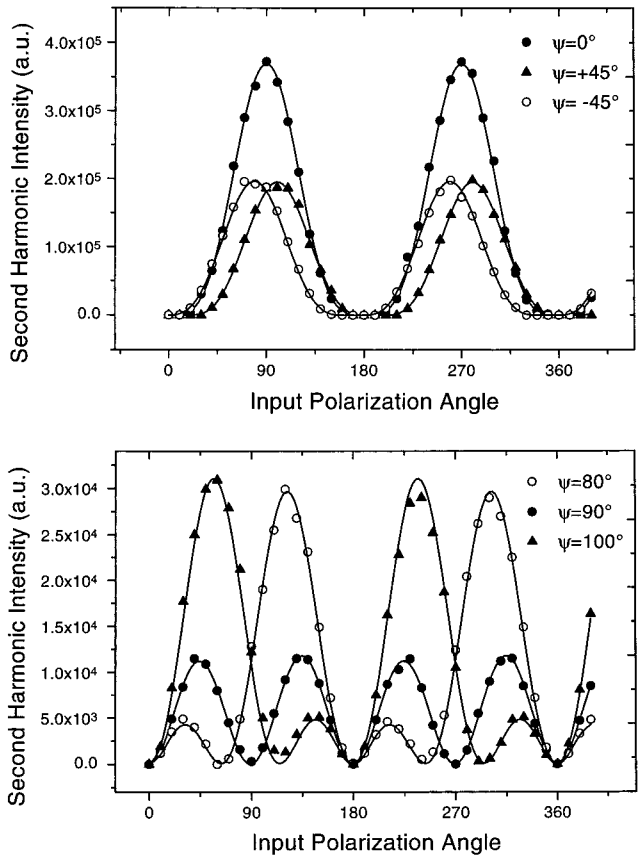

Figure 2. Polarized SH intensity versus input polarization angle obtained at 1.0 monolayer surface coverage and an SH polarization detection angle of (a, top) $\psi = 0°$ (p-polarization; filled circles), $\psi = \pm 45°$ (filled triangles and open circles, respectively) and (b, bottom) $\psi = 90°$ (s-polarization; filled circles), $\psi = 80°$ (open circles), and $\psi = 100°$ (filled triangles).

assumed isotropic distribution of molecules in the surface plane. Because the s-polarized SH intensity is proportional to the susceptibility component χ_{xzx}, the intensity maxima observed for incident polarization angles of 45°, 135°, 225°, and 315° have been used to determine the value of this tensor component via nonlinear least-squares fitting. Shown in Figure 2a is the incident polarization angle dependence of the p-polarized ($\psi = 0°$) SH response. The p-polarized SH response shows twofold symmetry. The intensity maxima observed for incident polarization angles of 90° and 270° are then used to obtain a value of the linear combination of susceptibility components χ_{xzx}, χ_{zxx}, and χ_{zzz}. For this determination, the value of χ_{xzx} is fixed at the value obtained from analysis of the s-polarized SH response. The values of χ_{zzz} and χ_{zxx} are then determined by a best fit of the data to eq 3 with the use of the nonlinear least-squares fitting algorithm.

It should be noted that under certain circumstances, the appearance of the polarized SH response curves can be extremely sensitive to the polarization purity of the fundamental fields as well as the output polarization angle. This is the case for the values of the MG susceptibility components presented here. The periodicity of the s-polarized SHG output (see Figure 2b) illustrates a particularly extreme example. Alignment accuracy to better than 0.2° of the SH analyzing polarizer was essential to obtain the results presented in Figure 2b ($\psi = 90°$). Deviations from pure s-polarized detection led to an alternation in intensity in adjacent maxima as illustrated and exaggerated by the $\psi = 80°$ and $\psi = 100°$ polarization curves also plotted in Figure 2b. Such an intensity asymmetry is often taken as evidence for additional nonzero susceptibility components contributing to the SH signal. Although this type of intensity pattern can be expected as an indicator of lower symmetry within the film and may result from a symmetry direction within the *XY* plane of the film[35] or from an isotropic distribution of chiral species,[36−38] care must be taken to ensure that the origin of the intensity alternation is not solely inadequate polarization selection. The fitting and analysis of intermediate polarization curves as illustrated in Figure 2 can preclude this possibility. For a narrow orientation distribution, the susceptibility parameters extracted from these SHG curves must be independent of polarization selection angle. The intermediate polarization curves provide a more stringent criterion for the fitting parameters, because all polarization curves must be adequately simulated by the same values of the $\chi^{(2)}_{IJK}$. The curves shown in Figure 2 have been fitted according to eq 3 and the susceptibility components extracted from the fits are listed in Table 1. The susceptibility components for each curve are averaged to provide a best-fit value and standard deviation for the set of five polarization curves.

Once obtained, the elements of the macroscopic nonlinear surface susceptibility tensor can be related to the components of the molecular nonlinear polarizibility tensor, β_{ijk}, to obtain the molecular orientation distribution function. This relation can be expressed as:

$$\chi_{IJK} = N_s \sum_{ijk} \langle l_{Ii} l_{Ji} l_{Kk} \rangle \beta_{ijk} \tag{5}$$

where N_s is the surface concentration of adsorbate molecules, l_{Ii} the direction cosine between the macroscopic (I) and molecular (i) Cartesian axes, and the brackets denote an orientational average over the N_s dye molecules on the surface. Figure 3 illustrates the molecular and surface reference frames and defines the angles necessary to simplify and evaluate the product of direction cosines that define the molecular orientation on the surface. In general, the orientation distribution function depends on the three angles θ, ϕ, and δ, which define the molecular and surface reference frames with respect to each other. However, because of the symmetry of the surface with respect to the azimuthal angle, ϕ, this function can be simplified by integration over all ϕ. This implies a random orientation of molecules about the surface normal.

The relevant nonlinear polarizability components necessary to solve eq 5 and determine the orientation function can be inferred from MG's electronic structure. Extensive examination of triphenylmethane dye electronic absorption and luminescence properties and their response to temperature and solvation changes has provided a detailed description of it's electronic state structure.[39−44] MG possesses two optically active, perpendicularly polarized bands in the visible region. The lower energy, x'-polarized, $S_1 \leftarrow S_0$ band appears at approximately 610 nm. At higher energy, at approximately 410 nm, lies the second excited electronic transition $S_2 \leftarrow S_0$, which, in our coordinate scheme, is z'-polarized (see Figure 3). The $S_2 \leftarrow S_1$ transition dipole is also x'-axis polarized. Thus, we consider contributions to the molecular polarizability from both $\beta_{x'x'z'}$ and $\beta_{z'x'x'}$ components. The use of 800 nm as a fundamental wavelength produces large nonlinear responses due to a two-photon resonance enhancement with the MG second excited electronic state. The wavelength dependence of the SH response shows that these enhancements are of order 300, indicating that $\beta_{z'x'x'}$ is approximately 15−20 times larger than $\beta_{x'x'z'}$. Substantial simplification of the orientation distribution function can be obtained by assuming only one dominant component of the

TABLE 1: Relative Second-Order Susceptibility Components and Averaged Orientation Angles Obtained via Nonlinear Least-Squares Fitting of Polarized SHG Intensity Data (See Text)

1.0 monolayer						
	$\psi = 0°, 90°$	$\psi = -45°$	$\psi = 45°$	$\psi = 80°$	$\psi = 100°$	average
χ_{xzx}	14.80	16.12	15.18	14.84	15.67	15.33 ± 0.58
χ_{zxx}	251.78	254.80	254.95	259.83	251.13	254.50 ± 3.44
χ_{zzz}	5.18	5.11	5.40	4.53	6.13	5.27 ± 0.48
$\xi = 84.4 \pm 0.5°$		$\xi = 8.2 \pm 0.5°$				
2.0 monolayers						
	$\psi = 0°, 90°$	$\psi = 45°$	average			
χ_{xzx}	8.38	2.78	5.58 ± 2.80			
χ_{zxx}	73.72	90.37	82.05 ± 8.32			
χ_{zzz}	2.92	5.85	4.39 ± 1.47			
$\xi = 81.1 \pm 2.0°$		$\theta = 13.2 \pm 3.1°$				
3.0 monolayers						
	$\psi = 0°, 90°$					
χ_{xzx}	-0.5					
χ_{zxx}	17.39					
χ_{zzz}	3.66					
$\xi = 72.6 \pm 5.0°$		$\theta = 25.9 \pm 5°$[a]				

[a] Errors estimated assuming ~10% uncertainty in susceptibility components.

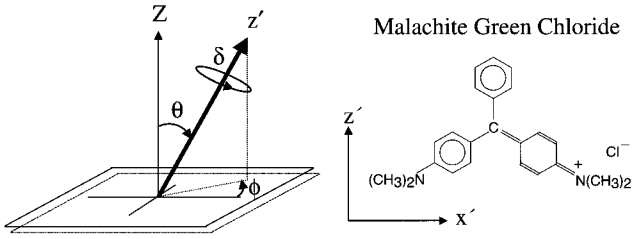

$$\chi^{(2)}_{IJK} = N \sum \langle l_{Ii'} l_{Jj'} l_{Kk'} (\phi,\theta,\delta) \rangle \beta_{i'j'k'}$$

Figure 3. MG and the definition of the molecular $x'y'z'$ coordinate system. Also shown are the definitions of the orientation angles θ, ϕ, and δ, defining the molecular orientation with respect to the surface *XYZ* reference frame.

polarizability tensor. Nevertheless, for the moment, we retain both contributions.

We have previously described the procedure for solving eq 5 with these two polarizability contributions and allowing for both the x' and y' molecular axes to be nonparallel to the surface.[9] This analysis yields an expression relating the ratio of the polarizability tensor components to the experimentally determined susceptibility components:

$$\frac{\beta_{x'x'z'}}{\beta_{z'x'x'}} = \frac{\chi_{zzz} + 2\chi_{xxz}}{\chi_{zzz} + 2\chi_{zxx}} \tag{6}$$

Using the experimentally determined susceptibility components listed in Table 1, eq 6 yields a ratio of $\frac{\beta_{z'x'x'}}{\beta_{x'x'z'}} = 14.3$, consistent with our earlier estimate based upon the magnitude of the resonance enhancement. The analysis also provides a condition defining the molecular orientation in terms of the orientation angle ξ, describing the angle that the x' molecular axis makes with the surface normal, expressed as a linear combination of the experimentally determined susceptibility components:

$$\langle \cos^2 \xi \rangle = \cos^2 \langle \xi \rangle = \frac{\chi_{zzz}}{2(\chi_{zzz} + \chi_{zxx} + \chi_{xxz})} \tag{7}$$

where we assume that all molecules possess the same averaged orientation angle. Using the measured susceptiblity components from Table 1, eq 7 yields an orientation angle of $\xi = 84.4 \pm 0.5°$. Although ξ can be determined unambiguously from the SHG measurements, the absolute molecular orientation cannot. The value of $\xi = 84°$ fixes the orientation of the x'-polarized transition dipole, but not how the molecule is oriented about this dipole. The absolute orientation requires specification of the angle θ to define the z'-polarized transition dipole direction.

To obtain an estimate of the value of θ and therefore specify the absolute molecular orientation, we can make use of the large difference in magnitudes of the susceptibility components. Given that $\beta_{z'x'x'}/\beta_{x'x'z'} = 14.3$, as determined from the measured susceptibility components, we now make the simplifying assumption that the molecular polarizability is dominated by $\beta_{z'x'x'}$ and neglect contributions from $\beta_{x'x'z'}$. Under these circumstances, the orientation angle θ, defining the z' molecular axis with respect to the surface normal, can be expressed in terms of the experimentally determined susceptibility components:[22]

$$\cos^2 \theta = \frac{2\chi_{ZXX} - \chi_{ZZZ}}{2\chi_{ZXX} + \chi_{ZZZ}} \tag{8}$$

Using the susceptibility components listed in Table 1, one obtains a value of $\theta = 8.2 \pm 0.5°$.

These results indicate that MG adopts an upright position on the surface with its x' molecular axis approximately perpendicular to the surface normal and its z' molecular axis possessing an averaged orientation angle close to the surface normal. This averaged orientation is consistent with MG interacting with the surface through its polar functional groups, as would be expected on the basis of simple physical arguments regarding the polar nature of the surface and of the MG dimethylamino substituents.

Similar analysis of the susceptibility components at different surface coverages can be used to obtain the averaged orientation in adjacent layers. The averaged orientation within the second molecular layer can be obtained by appropriate subtraction of the contribution of the first molecular layer. The susceptibility components and averaged orientation angles describing the second layer are also presented in Table 1. Use of eqs 7 and 8 for the second monolayer yield averaged orientation angles of $\xi = 81.1 \pm 2.0°$ and $\theta = 13.2 \pm 3.1°$. As expected from the appearance of the SH concentration dependence, MG adopts an orientation in the second adlayer that is very similar to that in the first molecular layer, with minor changes in the values of θ and ξ. The similarity in averaged orientation between the two layers is an interesting observation given that the orientation within the first layer appears to be dictated by the polar

interactions of the surface and the adsorbate functional groups. Completion of one monolayer may be expected to modify the surface characteristics and passivate its polar nature to some degree. We have recently used this rationale to explain the observation of antiparallel orientations in adjacent monolayers of R6G. In the case of R6G, however, the adsorbate possesses more polar substituents and as a result adopts a "flatter" orientation on the surface. The observation of similar orientations in the case of MG may indicate an interpenetration of the first and second monolayers, at least to the extent that molecules in the second adlayer are able to experience polar interactions similar to those experienced in the first monolayer. Nevertheless, film architectures with very similar orientations in adjacent layers are not uncommon and are occasionally encountered in film preparation using the Langmuir−Blodgett technique.[45,46]

Simpson and Rowlan have recently noted the danger in extracting orientation information from polarized SHG data.[47] They have argued that the assumption of a delta function angular distribution will result in inaccurate orientation angles when the distribution is broad. They have indicated that in the limit of very broad distributions, the average orientation angle extracted from SHG polarization measurements converge to a "magic angle" value of 39.2°, regardless of the mean angle of the distribution.[47] Thus, before attempting to extract orientation information from SHG measurements, knowledge of the breadth of the distribution is essential.

Here we present a method to address the breadth of the orientation distribution directly using the SH technique alone. The data presented in Figure 2 and Table 1 provide a measure of the SH response as a function of both the input and output polarization angles. The family of curves presented in Figure 2 represents the SH output polarization response. The data in Table 1 are the best-fit susceptibility components for each of the curves in Figure 2, as described. We argue that this analysis is a direct measure of the breadth of the orientation distribution. For a narrow (delta function) distribution in adsorbate orientation, one would expect to measure the same susceptibility components from each of the polarization curves obtained at different SH output polarization angle. That is, the output polarization dependence should obey eq 3 and the susceptibility parameters will be independent of the output detection angle, ψ. However, in the limit of a broad orientation distribution, changing the SH output detection polarization will produce a preferential sensitivity to different portions of the orientation distribution. The susceptibility components extracted from polarization curves obtained at different output detection angles will then reflect orientations that differ and show variation with detection polarization. Thus, susceptibility components characteristic of a broad distribution will be weighted by different components of the orientation distribution and show a corresponding variation as a function of the output detection polarization angle, reflecting the breadth of the distribution. Examination of Table 1 shows that all polarization curves obtained for the first monolayer can be fitted simultaneously with a narrow distribution of susceptibility parameters and therefore, must reflect a narrow distribution of orientations. It is also interesting to note that the fits for the second monolayer show more variation than those for one monolayer and therefore reflect a somewhat broader orientation distribution. Thus, it is unclear whether the averaged orientation angle reported for the second monolayer reflects a change in the mean of the orientation distribution or merely a change in its breadth.

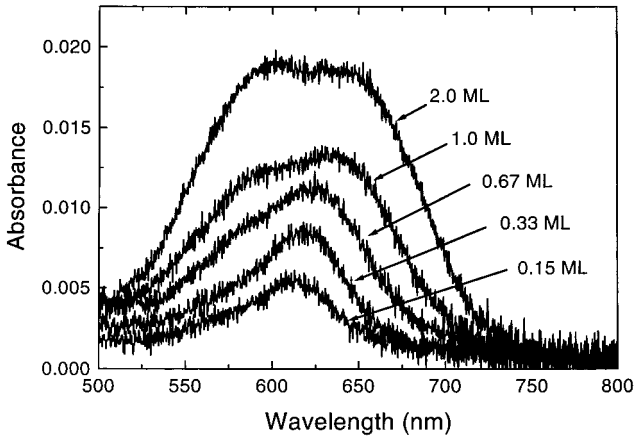

Figure 4. Optical absorbance spectra of MG films at surface coverages of 0.15, 0.33, 0.67, 1.0, and 2.0 monolayers (ML).

Polarization analysis for the third monolayer yields orientation angles of $\xi = 72.6 \pm 5.0°$ and $\theta = 25.9 \pm 5°$. In the absence of data at various polarization detection angles, it is difficult to determine whether this result reflects a significantly different orientation at this surface coverage (an approximate doubling in the angle that the z' molecular axis makes with the surface normal in comparison with its value in the first two molecular layers) or a broadening of the orientation distribution function. In either case, changes of this magnitude indicate a considerable difference in the nature of the adsorbate interaction, perhaps a reflection of more hydrophobic intermolecular interactions between adjacent molecular layers, distinct from those defining the averaged molecular orientation at lower surface coverages.

Absorbance Measurements. Figure 4 shows the optical absorbance spectra from MG-coated fused-silica surfaces. Absorbance versus wavelength plots are shown for five MG surface coverages, ranging in concentration from 0.15 to 2.0 monolayers, as determined through the SH concentration-dependence profiles. At the lowest surface coverage (0.15 monolayer), the spectrum shows an absorbance maximum at ∼615 nm. The spectrum is quite broad and slightly asymmetric, extending from approximately 670 nm in the red to 530 nm at its bluest. At one-third of one monolayer coverage the spectrum looks quite similar to that at lower coverage with the predominant changes being an overall increase in absorbance and a small shift in absorbance maximum by ∼10 nm to lower energy. At higher surface coverages (0.67 monolayer) these trends continue, showing a systematic red shift in absorbance maximum with increase in surface coverage. However, in addition to this red shift, the absorbance spectrum shows the onset of an absorbance feature that appears as a shoulder on the blue side of the absorption maximum at approximately 580 nm. Increasing the surface coverage to 1.0 monolayer gives rise to an additional red shift, but also the growth of the blue shoulder into a distinct, resolvable band with an absorbance maximum at approximately 590 nm. At a surface coverage of 2.0 monolayers, the blue feature, now with a wavelength maximum of 600 nm, has grown in intensity such that it is the predominant spectral feature and is easily resolved from the absorbance band appearing at 645 nm.

The observed spectral changes for MG are very similar to those observed in the case of R6G.[9] As discussed for R6G, we have attributed the systematic spectral red shift to changes in the polarity of the local surface environment and the growth in the blue spectral feature to the aggregation of adsorbate species. We have argued that the appearance of the blue spectral feature is related to the formation of sandwich-type aggregates with

parallel transition dipoles, consistent with the predictions of exciton band-splitting models of physical aggregation.[48−51] This geometry leads to the formation of two types of excited states: a higher-energy, optically allowed state with transition dipoles of the monomers aligned parallel to one another and a lower-energy, dipole-forbidden band with transition dipoles aligned antiparallel. These aggregates manifest themselves through absorbance features that are blue-shifted relative to the monomer bands. In addition, excitation of these sandwich-type aggregates is expected to lead to rapid radiationless decay from the higher-energy, blue-shifted band to the lower-energy, optically inactive band whose fluorescence is forbidden. Although our observations are consistent with this simple model, this description of the optical properties of these thin films is necessarily an oversimplification, and a complete understanding of the spectral characteristics must also include the role of the counterion in determining the local solvation effects and relative chromophore geometries.[43]

One important distinction between the observations for MG and R6G is the concentration at which appreciable levels of aggregation are observed. The onset of significant aggregation in the case of R6G occurs at a surface coverage of one monolayer and indicates the formation of interlayer aggregates, whereas significant levels of aggregation occur within the first monolayer of MG. The observation of intralayer aggregation in MG is not surprising in light of its upright orientation with respect to the surface. Similarly, R6G interacts primarily with the surface in its first monolayer and adopts a flatter orientation, making intralayer aggregation much less likely. Thus it appears that the averaged orientation and degree of aggregation in these ultrathin organic films is determined by the nature of the adsorbate−surface interactions and the molecular orientation that results, as well as the relative molecule−surface and intermolecular interaction strengths.

Attempts to measure fluorescence signals from MG-coated surfaces yielded no measurable signals. Although similar measurements on R6G monolayers gave rise to monomer fluorescence at low surface coverages and aggregate fluorescence at higher coverages, it is unclear whether the lack of a fluorescence signal in the case of MG results from similar aggregation effects as for R6G, or an immeasurable quantum yield due to rapid MG internal conversion dynamics. In their examination of MG surface dynamics using time-resolved SHG techniques, Morgenthaler and Meech[18] examined the coverage, wavelength, and intensity dependence of the ground-state recovery dynamics. They observed a fast component (∼15 ps) that was independent of all three experimental parameters and that they have attributed to the ultrafast isomerization dynamics similar to those observed in solution. In addition, an intensity- and coverage-dependent disruption of the film was observed on longer time scales and assigned to the multiphoton photochemistry of aggregates formed at high surface coverage. These observations would indicate that the lack of fluorescence is linked with the ultrafast dynamics; however it should also be noted that our orientation and absorbance measurements imply that significant levels of aggregation occur even at relatively low MG surface coverages and that aggregate-based fluorescence quenching cannot be ruled out entirely.

IV. Conclusion

Optical SHG has been used to probe the adsorbate−surface and adsorbate−adsorbate interactions of MG at the fused-silica/air interface. The concentration dependence of the SH response indicates the formation of ordered monolayers. Polarized SHG studies have provided the averaged molecular orientation in adjacent layers and a measure of the breadth of the orientation distribution function. MG adopts an upright orientation with its z' molecular axis near normal to the surface and its x' molecular axis approximately parallel to the surface. This orientation is consistent with the polar adsorbate−substrate interactions defined by the hydrophilic surface and the dimethylamino substituents of MG. Orientation in the second layer is very similar to that in the first monolayer, indicating that molecules in the second monolayer are still able to experience polar interactions with the surface or monolayer-modified surface. This may reflect an interpenetration of the first two adsorbate layers. Orientation in subsequent monolayers shows marked differences; however, it remains uncertain whether this is a result of MG adopting a flatter geometry, or simply a broadening of the orientation distribution function.

Aggregation effects are observed within the first monolayer and characterized by the onset of spectral features blue-shifted with respect to the monomer absorbance band. The formation of parallel, sandwich-type, *intralayer* aggregates is distinct from the *interlayer* aggregation observed between adjacent monolayers of rhodamine 6G. These differences are a direct result of the molecule−surface interactions that define their respective orientations in the first monolayer. Thus it appears that the order observed in the case of these ultrathin organic films is dictated by the molecule−surface interactions within the first monolayer as well as the magnitude of the intermolecular interactions in subsequent layers.

Acknowledgment. We thank the Natural Sciences and Engineering Research Council of Canada and Simon Fraser University for their financial support.

References and Notes

(1) Wu, A. P.; Kakimoto, M. A. *Adv. Mater*. (Weinheim, Ger.) **1995**, *7*, 812.
(2) DonatBouillud, A.; Mazerolle, L.; Gagnon, P.; Goldenberg, L.; Petty, M. C.; Leclerc, M. *Chem. Mater*. **1997**, *9*, 2815.
(3) Ostergard, T.; Paloheimo, J.; Pal, A. J.; Stubb, H. *Synth. Met.* **1997**, *88*, 171.
(4) Rikukawa, M.; Nakagawa, M.; Abe, H.; Ishida, K.; Sanui, K.; Ogata, N. *Thin Solid Films* **1996**, *273*, 240.
(5) Paddeu, S.; Ram, M. K.; Nicolini, C. *J. Phys. Chem. B* **1997**, *101*, 4759.
(6) Agbor, A. E.; Petty, M. C.; Monkman, A. P. *Sens. Actuators, B* **1995**, *28*, 173.
(7) Paloheimo, J.; Kuivalainen, P.; Stubb, H.; Vuorimaa, E.; Yli-Lahti, P. *Appl. Phys. Lett.* **1990**, *56*, 1157.
(8) Paloheimo, J.; Stubb, H.; Vuorimaa, E.; Yli-Lahti, P.; Dyreklev, P.; Inganas, O. *Thin Solid Films* **1992**, *210*, 283.
(9) Kikteva, T.; Star, D.; Zhao Z.; Baisley, T. L.; Leach, G. W. *J. Chem. Phys. B* **1999**, *103*, 1124.
(10) Sundstrom, V.; Gillbro, T.; Bergstrom, H. *Chem. Phys.* **1982**, *73*, 439.
(11) Lewis, G. N.; Magel, T. T.; Lipkin, D. *J. Am. Chem. Soc.* **1942**, *64*, 1774.
(12) Erskine, D. J.; Taylor, A. J.; Tang, C. L. *J. Chem. Phys.* **1984**, *80*, 5338.
(13) Ippen, E. P.; Shank, C. V.; Bergman A. *Chem. Phys. Lett.* **1976**, *38*, 611.
(14) Ben-Amotz, D.; Harris, C. B. *J. Chem. Phys.* **1987**, *86*, 4856.
(15) Gottfried, N. H.; Roither, B.; Scherer, P. O. J. *Opt. Comm.* **1997,** *143*, 261.
(16) Meech, S. R.; Yoshihara, K. *J. Phys. Chem*. **1990**, *94*, 4913.
(17) Meech, S. R.; Yoshihara, K. *Chem. Phys. Lett.* **1990**, *174*, 423.
(18) Morganthaler, M. J. E.; Meech, S. R. *Chem. Phys. Lett.* **1993**, *202*, 57.
(19) (a) Shen, Y. R. *Annu. Rev. Phys. Chem.* **1989**, *40*, 327. (b) Shen, Y. R. *Nature* **1989**, *337*, 519.
(20) Richmond, G. L.; Robinson, J. M.; Shannon, V. L. *Prog. Surf. Sci.* **1988**, *28*, 1.
(21) Eisenthal, K. B. *Annu. Rev. Phys. Chem.* **1992**, *43*, 627.

(22) Corn, R. M.; Higgins, D. A. *Characterization of Organic Thin Films*; Ulman, A., Ed.; Butterworth-Heinemann: Boston, 1995; Chapter 12.

(23) Higgins, D. A.; Byerly, S. K.; Abrams, M. B.; Corn, R. M. *J. Phys. Chem*. **1991**, *95*, 6984.

(24) Higgins, D. A.; Abrams, M. B.; Byerly, S. K.; Corn, R. M. *Langmuir* **1992**, *8*, 1994.

(25) Campbell, D. J.; Higgins, D. A.; Corn, R. M. *J. Phys. Chem*. **1990**, *94*, 3681.

(26) Kemnitz, K.; Bhattacharyya, K.; Hicks, J. M.; Pinto, G. R.; Eisenthal, K. B. *Chem. Phys. Lett.* **1986**, *131*, 285.

(27) Conboy, J. C.; Daschbach, J. L.; Richmond, G. L. *J. Phys. Chem*. **1994**, *98*, 9688.

(28) Naujok, R. R.; Higgins, D. A.; Hanken, D. G.; Corn, R. M. *J. Chem. Soc., Faraday Trans.* **1995**, *81*, 1411.

(29) Grubb, S. G.; Kim, M. W.; Rasing, T.; Shen, Y. R. *Langmuir* **1988**, *4*, 452.

(30) Bloembergen, N.; Pershan, P. S. *Phys. Rev.* **1962**, *128*, 606.

(31) Cnossen, G.; Drabe, K. E.; Wiersma, D. A. *J. Chem. Phys.* **1992**, *97*, 4512.

(32) Ye, P.; Shen, Y. R. *Phys. Rev. B.* **1993**, *28*, 4288.

(33) Felderhof, B. U.; Bratz, A.; Marowsky, G.; Roders, O.; Sieverdes, F. *J. Opt. Soc. Am. B* **1993**, *10*, 1824.

(34) Mizrahi, V.; Sipe, J. E. *J. Opt. Soc. Am. B* **1988**, *5*, 660.

(35) Chen, W.; Feller, M. B.; Shen, Y. R. *Phys. Rev. Lett.* **1989**, *63*, 266.

(36) Petralli-Mallow, T.; Wong, T. M.; Byers, J. D.; Yee, H. I.; Hicks, J. M. *J. Phys. Chem.* **1993**, *97*, 1383.

(37) Byers, J. D.; Yee, H. I.; Hicks, J. M. *J. Chem Phys.* **1994**, *101*, 6233.

(38) Verbiest, T.; Kauranen, M.; Maki, J. J.; Teerenstra, M. N.; Schouten, A. J.; Nolte, R. J. M.; Persoons, A. *J. Chem. Phys.* **1995**, *103*, 8296.

(39) Lueck, H. B.; McHale, J. L.; Edwards, W. D. *J. Am. Chem. Soc.* **1992**, *114*, 2342.

(40) Grocock, D. E.; Hallas, G.; Hepworth, J. D. *J. Chem. Soc., Perkin Trans. 2* **1973**, *3*, 1166.

(41) Duxbury, D. F. *Chem. Rev.* **1993**, *93*, 381.

(42) Yoshizawa, M.; Suzuki, K.; Kubo, A.; Saikan, S. *Chem. Phys. Lett.* **1998**, *290*, 43.

(43) Korppi-Tommola, J.; Yip, R. W. *Can. J. Chem.* **1981**, *59*, 191.

(44) Korppi-Tommola, J.; Kolehmainen, E.; Salo, E.; Yip, R. W. *Chem. Phys. Lett.* **1984**, *104*, 373.

(45) Roberts, G. *Langmuir*−*Blodgett Films*; Plenum: New York, 1990.

(46) Petty, M. C. *Langmuir*−*Blodgett Films: An Introduction*; Cambridge University Press: Cambridge, U.K., 1996.

(47) Simpson, G.; Rowlan, K. *J. Am. Chem. Soc.* **1999**, *121*, 2635.

(48) McRae, E. G.; Kasha, M. *J. Chem Phys*. **1958**, *28*, 721.

(49) Hochstrasser, R. M.; Kasha, M. *Photochem. Photobiol*. **1964**, *3*, 317.

(50) Kasha, M.; Rawls, H. R.; El-Bayoumi, M. A. *Pure Appl. Chem*. **1965**, *11*, 371.

(51) Pope, M.; Swenberg, C. E. *Electronic Processes in Organic Crystals*; Oxford University Press: New York, 1982; Chapter 1D.